Model Independent Numerical Procedure for the Diagonalization of a Multiple Input Multiple Output Dynamic System

Gianluca Persichetti, Antonino Chiummo, Fausto Acernese, Fabrizio Barone, Rosario De Rosa, Fabio Garufi, Leopoldo Milano, and Simona Mosca

***Abstract*—Seismic noise limits Earth based gravitational wave interferometric detectors at low frequencies. The detection threshold can be lowered down to a few Hz using a seismic attenuation system based on Inverted Pendulum (IP) which sustains interferometer optical components by means of a chain of pendulums. The IP, acting as a mechanical low pass filter, is able to filter out seismic noise in the horizontal plane and at the same time it provides a quasi-inertial stage where the suspension point of the chain of pendulums lies.**

The main degrees of freedom of an IP are three: two translational modes and one rotational mode. Therefore, to fully determinate its position, three independent sensors are mounted at the periphery of the IP top table. For the same reason, three independent actuators are used to move the IP. The geometrical position of the sensors is different from actuator positions, in addition, both of them are not connected to the normal modes of the IP. Each sensor will be sensitive in all the three IP normal modes and each actuator will generate movements which are a mix of the three modes. To take advantage of controlling a Single Input Single Output (SISO) system instead of a Multiple Input Multiple Output (MIMO) system, a diagonalization of the actuation and detection system is needed. An original and model independent experimental procedure for determining the system dynamics, giving an effective diagonalization has been developed and tested.

***Index Terms*—Diagonalization, multiple input multiple output systems, sensor and actuators.**

I. Introduction

THE model design of a MIMO system is often a difficult task. For instance a typical problem is related with a possible disagreement between measured response and the model estimation, especially in cases where the model depends on many parameters that cannot be precisely determined by means of measurements.

Manuscript received June 14, 2010; revised April 28, 2011; accepted May 26, 2011. Date of publication July 22, 2011; date of current version August 17, 2011. This work was supported by the Italian Ministero dell'Università e della Ricerca under the PRIN 2007 Research Program Framework.

F. Acernese and F. Barone are with the Università degli studi di Salerno, 84034 Fisciano SA, Italy, and also with the INFN Sezione di Napoli, Napoli, Italy (e-mail: fausto.acernese@na.infn.it; fabrizio.barone@na.infn.it).

R. De Rosa, F. Garufi, L. Milano, S. Mosca, and G. Persichetti are with the Università degli Studi di Napoli Federico II, Napoli, Italy, and also with the INFN Sezione di Napoli, Napoli, Italy (e-mail: rosario.derosa@na.infn.it; fabio.garufi@na.infn.it; leopoldo.milano@na.infn.it; simona.mosca@na.infn.it; gianluca.persichetti@gmail.com).

A. Chiummo is with the European Gravitational Observatory, 56021 Cascina, Italy (e-mail: antonino.chiummo@ego-gw.it).

Digital Object Identifier 10.1109/TNS.2011.2159846

When possible, decoupling multiple input and output channels into several independent single input and output channels can be considered a classical procedure in control system design.

In the following we will consider a procedure to transform a multivariable mechanical system into a set of single input single output system. As we will describe, this method was born in the framework of the control system design in suspended gravitational wave interferometers [1]–[4], but obviously the procedure can be applied on different physical systems.

Let suppose our system to be linear and stationary. This means that when we will apply the numerical procedure to actual physical systems we will restrict our consideration only where their dynamical range has a linear behavior.

Let us suppose that the system is equipped with n sensors and n actuators respectively capable to sense and actuate on the main n normal modes.

The input vector $\mathbf{c} = (c_1, c_2, \ldots, c_n)$ represents the signals sent to the actuators whereas the output vector $\mathbf{l} = (l_1, l_2, \ldots, l_n)$ is the signal provided by the sensors.

If the n normal modes of the system are not orthogonal to the sensitivity axis of the sensors, each sensor should be sensitive to the projections of all normal modes on its axis. In the same way, each actuator will generate movements that are a mix of system modes.

Here and in the following, the word *diagonalization* means the procedure to obtain a new sensor/actuator space in which each normal mode is independently sensed. In this *virtual* space it will be possible also to actuate on a specific normal mode.

From the mathematical point of view, it should be mentioned that it is not always possible converting a system from MIMO to SISO as explained for instance in [5].

To diagonalize the system means to find a suitable linear combination of the sensor outputs (*virtual sensors*) each sensitive to a single normal mode. In the same way as *virtual actuators* we intend a linear combination of the actuator signals which is able to excite a single normal mode of the system. Before the diagonalization we can consider our system a MIMO system. The diagonalization procedure allows to consider our system as composed of many SISO systems.

The reason to prefer a SISO system is that a single degree of freedom system is often much easier to control: each mode is controlled by means of an independent feedback loop, simplifying the overall loop design.

As it will be shown, using this method we just require the system to be linear and stationary with the same number of inputs and outputs. This point makes such a procedure very flexible and suitable to be applied in different physical systems.

II. The Seismic Attenuation System

The purpose of the VIRGO experiment is to detect gravitational waves produced by astrophysical sources in a frequency range between 10 Hz and some kHz. VIRGO is the unique interferometric detector capable to detect signals below 50 Hz and one of its main goals is to extend the low frequency detection threshold down to a few Hz (to enlarge the potentially detectable sources number). In this frequency range, the seismic noise limits the detector sensitivity. One of the most efficient Seismic Attenuation System (**SAS**) for gravitational waves interferometers is a chain of pendulums, suspended from a very low-frequency stage called *Inverted Pendulum* [6]. Each optical component of the interferometer is supported by means of this particular suspension system. In the Naples VIRGO laboratory a simplified prototipe of this interferometric detector is available. Thanks to this small interferometer it will be possible to develop and test new sensors and new control systems to employ for the VIRGO interferometer.

The seismic vibrations of the ground are many orders of magnitude greater than the displacements we need to detect.

Measurements of seismic noise at frequencies > 0.5 Hz have been carried out by many groups [7]–[9]. Above some Hz, the spectrum of seismic vibrations is well approximated by the empirical expression:

$$\tilde{x}_t = \frac{a}{f^2}\frac{m}{\sqrt{Hz}} \tag{1}$$

where f is the frequency and a is a constant varying in the range $10^{-9} < a < 10^{-6}$ depending on sites.

Considering that the length variation induced by a gravitational wave is less than 10^{-18} m, with a ground motion amplitude around 10^{-6} m, the required attenuation factor should be at least 10^{-12}.

For this reason we need a very efficient seismic attenuation system. The simplest seismic filter we can consider is a simple pendulum. A pendulum is a harmonic oscillator of natural frequency:

$$f_0 = \frac{1}{2\pi}\sqrt{\frac{g}{L}} \tag{2}$$

where L is the pendulum length. It acts as a low-pass mechanical filter with the following response:

$$T(f) = \frac{f_0^2}{f^2 - f_0^2 + \frac{if_0 f}{Q}} \tag{3}$$

being Q is the quality factor of the pendulum. It is clear that:

- At low frequencies $f \ll f_0$ the pendulum is a short circuit for ground vibrations.
- At high frequencies $f \gg f_0$ the ground motion is attenuated.

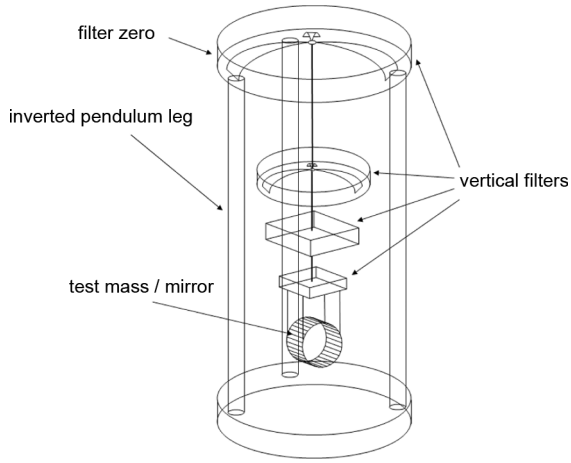

Fig. 1. Seismic Attenuation System used to test the numerical procedure. The horizontal seismic attenuation is achieved by means of the inverted pendulum. The vertical attenuation is performed by means of filters based on linear anti-spring effect [10].

In order to achieve a suitable attenuation factor, several pendulums are chained. This is the reason why in the VIRGO interferometer (and in the Naples interferometer too) all the optical components are suspended by means of a chain of pendulums.

Theoretically, just the seismic oscillation along the interferometer optical axis should have some practical effect. But in the real systems, the motion in all the degrees of freedom must be attenuated because of the unavoidable coupling between translational and rotational components. This means, for instance, that a vertical displacement (which is ineffective for a plane mirror interferometer) has effect also along the beam direction; moreover, cross-couplings between vertical and horizontal (longitudinal) oscillations potentially limit the performance of mechanical isolation systems.

The whole attenuation system is composed by 5 stages (see Fig. 1). Schematically, we can describe our system in terms of four elements:

- the pre-isolation stage (the *inverted pendulum*);
- the vertical filters;
- the chain of pendulums;
- the mirror.

The vertical isolation is achieved, in our system, by means of Monolithic Geometric Anti-Spring filters (MGAS) (see for instance [10]). The MGAS, based on linear anti-spring effect, is a set of radially arranged cantilever springs, mounted from a common retainer ring structure and opposing to each other via a central disk. The payload to be isolated (the chain of pendulums) is connected to the central part.

Such a solution realizes low frequency resonance, typically about a few hundreds of mHz

In the following we will briefly describe the *inverted pendulum* and the way to control the mirror.

A. The Inverted Pendulum

The interferometer optical elements (mirrors and beam splitter) and the chain of pendulums are sustained by means of a very low frequency stage: the *Inverted Pendulum*. This stage

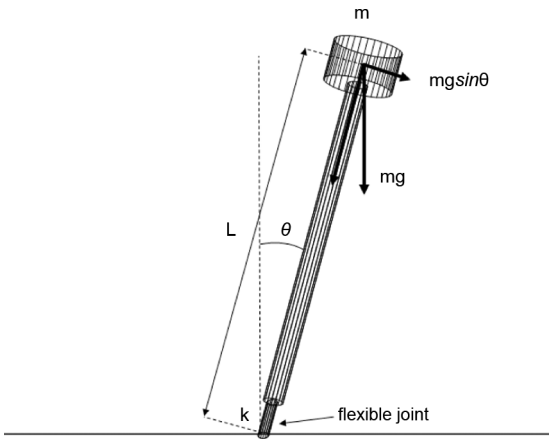

Fig. 2. The inverted pendulum is the element on which is based the horizontal seismic attenuation system. In a simplified model it can be described as a rigid massless rod with length L and mass M, supported by means of a perfectly elastic element having spring constant κ.

itself is an oscillator but its resonance frequencies are lower than the resonance frequencies of the chain of pendulums. The IP is composed of three flexible joints, each supporting a leg. At the top, the three legs are connected to a rigid table by means of small flexures. Such a rigid table is called *Filter Zero* (**F0**). It is a vertical filter which uses blades to suspend the chain of pendulums.

The IP has a triple function:

- pre-filtering low frequency seismic noise, providing attenuation at frequencies of microseismic peak;
- providing a quasi-inertial stage to actively damp the motion of the suspended chain, avoiding actuation noise re-injection (taking advantage of the passive attenuation between the IP itself and the test mass);
- providing a mean to allow precision positioning of the mirror and the chain of pendulums using small forces.

The IP is a three degrees of freedom system. It has two translational modes and one torsional mode. An inverted pendulum can be described, in a simplified model, as a rigid massless rod having length L and mass M, supported by a perfectly elastic element having spring constant κ, as it is shown in Fig. 2.

The motion equation is

$$I\ddot{\theta} = -\kappa\theta + mgL\sin\theta \tag{4}$$

where θ is the angle between the vertical axis and the rod whereas I is the IP momentum of inertia with respect to the suspension point. The term $mgL\sin\theta$ is the torque acting on mass due to gravity, which tends to pull the rod away from the vertical position, and is $\approx mgL$ (in the small-angle approximation). The restoring force from the flexure is $-\kappa\theta$. The full torque acting on the rod is $N_{ext} = -(\kappa - mgL)\theta$.

In the small angle approximation we can write the (4) as

$$I\ddot{\theta} = -\kappa_{eff}\theta \tag{5}$$

where $\kappa_{eff} = \kappa - mgl$ is the effective spring constant acting as an antispring is able to reduce the overall stiffness.

If the (4) is rewritten in terms of the linear displacement measured on the top of the IP $x = \theta l$ and introducing the linear stiffness $k = \kappa/l^2$, solving in the frequency domain, we can find the IP resonance angular frequency ω, which is given by

$$\omega^2 = \frac{\kappa - mgL}{I}. \tag{6}$$

One of the advantage in using an IP is the easy way to control it. In fact, the force needed to move the IP of the amount x ($x = \theta L$) at frequencies lower than the resonant frequency is something like $F \sim M\omega^2 x$. Assuming a mass of the order of 1 ton and a resonant frequency of 30 mHz, only 0.36 N are required to move the IP top of 1 cm.

As previously mentioned, on the top of the IP there is the *Filter Zero* where is placed the suspension point of the chain of pendulums.

The *Filter Zero* is actively controlled. The reason to control actively the system is the following: the attenuation system elements described until now and the results they are able to obtain are not sufficient to match the locking requirements. Each element provide a passive filtering out. In particular:

$f < IP\ resonance\ frequency$. The seismic noise is completely transmitted to the mirror (because no filter is present). In the VIRGO case the displacement produced by tidal effects can be even 60 μm.

$IP\ resonance\ frequency < f < some\ Hz$. Normal modes of the attenuation system itself (IP and chain of pendulums elements) are responsible of mirror oscillation that in the VIRGO case can exceed 10 μm}

In both cases amplitude oscillation exceeds design limit for several orders of magnitude (8 in the VIRGO case). The solution is offered by an *active* control. This control should not act directly on the mirror because the amplitude attenuation to perform is too expensive (in terms of dynamical range). This is the reason why the control is realized in a hierarchical way [11] in different points of the system and each control acting at its competence bandwidth. In our system those points are:

The inverted pendulum. Thanks to its peculiar structure it is possible obtaining displacement of ± 1 cm in the frequency range $f < 0.1$ Hz without injecting electronic noise.

The intermediate stage. On this element is possible to apply forces which produce displacement of ± 10 μm in the bandwidth 0.1–1 Hz.

The mirror. For f $>$ 1 Hz forces can be applied directly on the reference mass which holds the mirror.

III. Sensors and Actuators System

The framework where the diagonalization idea was born is the control system development in suspended gravitational wave interferometers [16], [17] . In particular this procedure was used on the position control of the *Filter Zero*. Before to use the procedure on a complex system, we tested the method on a simpler system. In the following we will describe the sensors and actuators system on which the procedure has been applied.

A. Sensors and Actuators on Simple Pendulum

The preliminary testing bench was a system very similar to the last stage of the chain of pendulums: a mirror suspended by means of a simple pendulum.

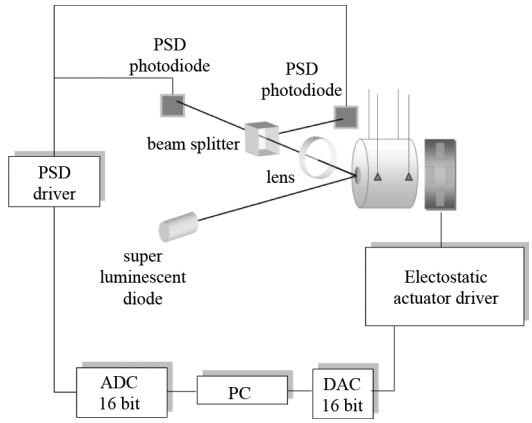

Fig. 3. System composed by electrostatic actuators and optical lever used to additionally test the diagonalization procedure. If the PSDs are placed in the focal plane of the lens or in the conjugate point of the mirror, they detect only the tilt or the translation of the mirror respectively. In the experimental setup, the PSDs were not placed in this configuration, so that each photodiode senses both tilt and translation.

This experimental setup is used to test electrostatic actuation instead of the magnet coil actuation presently used in the VIRGO interferometer. Electrostatic actuators (**EA**) [14] are promising devices for mirror control in next generation interferometric gravitational wave detectors.

In the system depicted in Fig. 3 the mirror position is detected using an optical lever: light from a superluminescent diode is sent through a single-mode optical fibre to the mirror. The reflected beam is detected by means of a position sensing photodiode (PSD).

In this case the main degrees of freedom of the mass/mirror system are: a translational mode and a rotational mode (with respect to the vertical). Electrostatic actuators are used to excite the mass. The reflected optical beam is split by means of a beam splitter and a lens is used to perform a preliminary uncoupling of the two degrees of freedom as described in [13]. Two PSDs receive the optical signals carrying information on tilt and translation of the suspended mass/mirror.

B. Sensors and Actuators on the Inverted Pendulum

On the *Filter Zero* a set of sensors and actuators are mounted. A triplet of *linear variable differential transformer* (**LVDT**) [12] that are high-precision position sensors is mounted in a triangular configuration at the edge of *Filter Zero* plate.

Such position transducers have been expressly designed to this purpose. An LVDT is composed by a primary and two secondary windings. The moving central coil (*the exciter*) is driven by a 20 kHz signal; the two secondary coils, symmetric with respect to the primary, are in series and oppositely wound. A displacement of the exciter induces current changes in the windings proportional to the displacement amplitude. The signal from the receiver is amplified, then demodulated in phase and low-pass filtered. They are low-power, ultra-high-vacuum compatible, non contacting position sensor with nanometer resolution and centimeter dynamic range.

LVDTs are used to measure the relative motion of the IP with respect to the ground. For this purpose the exciter is mounted on the *Filter Zero* and the secondary coils are connected to an external frame (mechanically connected to the ground).

The horizontal actuation system is realized by a triplet of magnet-coil actuators [15]. They are composed by a couple of coils and a central magnet. The magnet coil is orthogonal to the coil axis and a current passing through the coil generates a proportional force.

As happens for position sensors, the windings are connected to the *Filter Zero* and magnets are placed on the external frame. Actuators are mounted in a triangular configuration as the LVDT but, for practical reason, not in the same position.

The sensor and actuator signal are processed by a 16 bit *analog-to-digital converter* (**ADC**) a *central processing unit* (**CPU**) and a 16 bit *digital-to-analog converter* (**DAC**). The CPU handles all sensors and actuators signals and recombines them using matrices. In this way is possible to create complex feedback filters with high pole/zero placement precision and perform calculation with a sampling frequency of 4 kHz.

IV. The Diagonalization Method

The diagonalization procedure has been conceived to help the control system design of the *Filter Zero* position described previously.

The method described in this section can be used on linear and stationary systems and is effective in extracting their normal modes. It is based on the measure of the transfer function matrix and on the possibility to express it in diagonal form.

To this purpose we will describe the diagonalization method in a general way. It will be easy to express the terms of the procedure on a different physical system.

Let consider n generic actuators that are able to excite the system. Their signals are represented by means of the vector $\mathbf{c} = (c_1, c_2, \ldots, c_n)$. Moreover let consider n detectors signals $\mathbf{l} = (l_1, l_2, \ldots, l_n)$ that give a measure of the response of the system.

What we want is to make the system *diagonal* i.e., write down the right linear combination of sensor signals to obtain *virtual* uncoupled detector signals $\mathbf{l}^{virt} = (l_1^{virt}, l_2^{virt}, \ldots, l_n^{virt})$. Furthermore, we would like to write down the right linear combination of *real* actuator signals to obtain *virtual* actuators $\mathbf{c}^{virt} = (c_1^{virt}, c_2^{virt}, \ldots, c_n^{virt})$ capable to act on a single degree of freedom at a time.

In other words the condition we wish to obtain is

$$\mathbf{l}^{virt} = \mathcal{H} \cdot \mathbf{c}^{virt}.$$

As depicted in detail in Fig. 5:

But the starting situation is

$$\mathbf{l} = \mathcal{R} \cdot \mathbf{c}$$

where the matrix $\mathcal{R}_{ij}(s)$ is composed by the experimental transfer functions obtained exciting the system by means of the ith real detector and detecting signals using the jth real actuator.

We define the sensing matrix $\mathcal{S}_{ki}$ as the matrix which describes the coupling of the kth virtual detector with the ith real detector:

$$\mathbf{l}^{virt} = \mathcal{S} \cdot \mathbf{l}$$

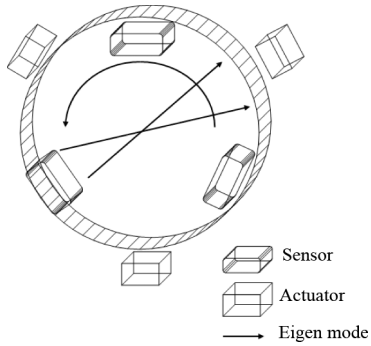

Fig. 4. Simplified scheme of sensors and actuators system placed on the Filter Zero (top view). The main eigen modes of the inverted pendulum are two translational mode and one rotational mode.

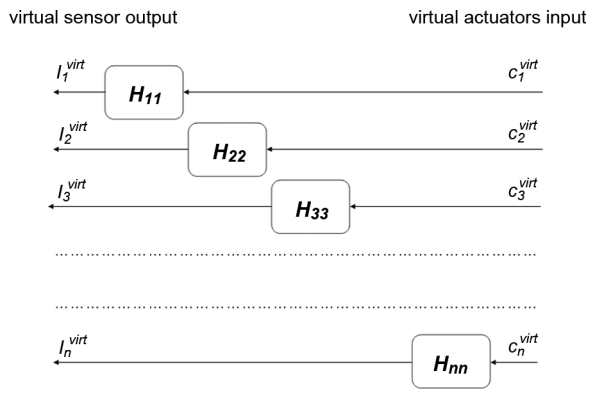

Fig. 5. Diagonalization goal: each actuator is able to excite a specific mode that is detected by means of a specific sensor.

The driving matrix $\mathcal{D}_{jk}$ describes the coupling of the jth real actuator with the kth virtual actuator and it is defined as

$$\mathbf{c} = \mathcal{D} \cdot \mathbf{c}^{virt}.$$

So the overall transfer function of virtual detectors over virtual actuators can be written as follows:

$$\mathbf{l}^{virt} = \mathcal{S} \cdot \mathcal{R}(s) \cdot \mathcal{D} \cdot \mathbf{c}^{virt}$$

or

$$\mathbf{l}^{virt} = \mathcal{H} \cdot \mathbf{c}^{virt}$$

where we can identify

$$\mathcal{H} = \mathcal{S} \cdot \mathcal{R}(s) \cdot \mathcal{D}. \tag{7}$$

The goal is to estimate the sensing matrix $\mathcal{S}$ and the driving matrix $\mathcal{D}$ from experimental data $\mathcal{R}_{ij}(s)$. The transfer function matrix $\mathcal{R}_{ij}(s)$ is experimentally evaluated exciting with white noise the system by means of the actuator c_j and detecting the response l_i of the ith sensor $(i = 1, 2, \ldots, n)$. For each excitation we can detect a row of $R_{ij}(s)$. This means that to fully determine $\mathcal{R}_{ij}(s)$ we need to excite n times our system building the response matrix row by row.

Several approaches have been used for this purpose [16]–[18]. Our method is very simple in principle: we estimate $\mathcal{S}$ and $\mathcal{D}$ building the matrix function $\mathcal{H} = \mathcal{S} \cdot \mathcal{R}_(s) \cdot \mathcal{D}$ which have to be in a diagonal form.

Using a mathematical algorithm, we look for the $\mathcal{S}$ and $\mathcal{D}$ which are able to minimize all off diagonal elements.

This algorithm has been implemented in a *Matlab*® code using, as solver, the *lsqnonlin* library function, designed for nonlinear least-squares minimization [19].

Lsqnonlin manages function whose sum of squares is minimized. In our case, we minimize the function consisting in the sum of the squared off-diagonal elements $\sum_{lk} |\mathcal{H}_{lk}|^2$ where $l \neq k$.

Furthermore we request the transformation matrices to have some additional condition to avoid to find trivial solution only. We request the normalization of each row of $\mathcal{S}$ (such a condition will preserve also measurement units in the virtual sensors) and the the normalization of each row of the inverse of $\mathcal{D}$ (which is the matrix we want to preserve measurement units). In order to implement those requirements we have to minimize the quantity:

$$\sum_{lk} |\mathcal{H}_{lk}|^2 + w[(\mathcal{S} \cdot \mathcal{S}^T - 1)^2 + (\mathcal{D}^{-1} \cdot (\mathcal{D}^{-1})^T - 1)^2] \tag{8}$$

where $l \neq k$, w is an arbitrary weight and the second term $[(\mathcal{S} \cdot \mathcal{S}^T - 1)^2 + (\mathcal{D}^{-1} \cdot (\mathcal{D}^{-1})^T - 1)^2]$ corresponds to the required normalization condition. The reason to insert w in the quantity to minimize (8) is justified because of the extreme unbalancing in the sum between the terms $\sum_{lk} |\mathcal{H}_{lk}|^2$ (whose number is related to the frequency range considered) and the single term $[(\mathcal{S} \cdot \mathcal{S}^T - 1)^2 + (\mathcal{D}^{-1} \cdot (\mathcal{D}^{-1})^T - 1)^2]$. We have chosen w equal to the number of measured data in order to balance the weight between the two terms in the (8).

V. The Diagonalization Results

The preliminary tests have been performed on the simple pendulum previously described. In this case the signals we send to EA are EA_R and EA_L (we use only two horizontal electrodes among four available electrodes stripes). Electrostatic actuators excite the suspended mass and two PSDs detect mirror movements. Exciting one electrode at time using white noise we are able to measure $R_{ij}(s)$.

An example of real transfer function is shown in Fig. 7 and the sensing matrix found is

$$\mathcal{S} = \begin{pmatrix} 0.9975 & 0.0702 \\ -0.1856 & 0.9826 \end{pmatrix}. \tag{9}$$

At the same time the procedure found the driving matrix:

$$\mathcal{D} = \begin{pmatrix} 0.6211 & 0.6403 \\ 0.8275 & -0.8128 \end{pmatrix}. \tag{10}$$

Taking into account the previous matrices (9) and (10) it is possible to build virtual sensor signals and virtual actuator signals. Applying those results on our system it has been possible to uncouple the degrees of freedom, as shown in Fig. 8.

Table I reports the upper and lower limits for the elements of the simple pendulum $\mathcal{S}$ and $\mathcal{D}$ matrices corresponding to the 95% confidence level, estimated by using the *nlcparci Matlab*® function [20].

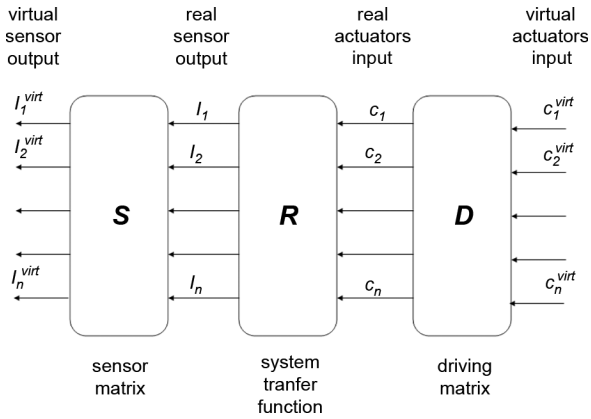

Fig. 6. Matrix definition: $\mathcal{S}$ is the sensing matrix, $\mathcal{R}$ is the system transfer function and $\mathcal{D}$ is the driving matrix.

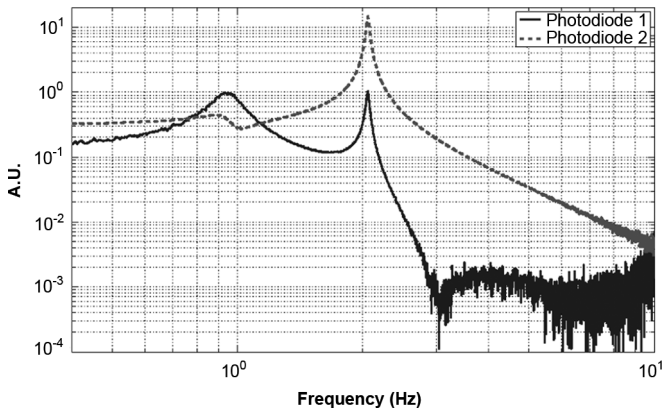

Fig. 7. Transfer functions obtained exciting the mirror using the horizontal electrodes of the EA. In particular the transfer function in the figure is referred to the right electrode.

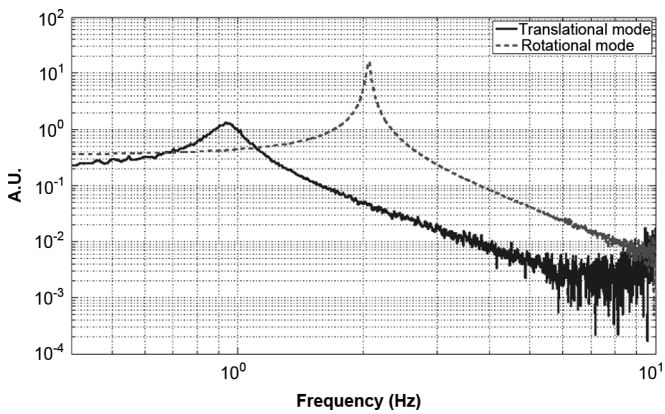

Fig. 8. Diagonalized transfer function in the optical lever system. This plot is the superposition of two different experimental transfer function obtained exciting the system by means of each virtual actuator and detecting by means the corresponding virtual detector.

After the preliminary tests on a single stage pendulum, the procedure has been applied on a more complex system: the IP previously described.

In this case, LVDT are the sensors used to detect the IP motion and magnet-coil systems are the actuators. Each sensor should be sensitive to movements in all three IP normal modes. In the same way, each actuator will generate movements of the IP involving a mix of the three modes. In the following we will call the IP normal modes x, z and ty although they do not correspond necessarily to orthogonal translations and a rotation. If the system would have been perfectly symmetrical, we would notice a degeneration in the translational modes. In a real system the two translational modes are quasi-degenerate.

TABLE I
UPPER AND LOWER LIMITS FOR THE ELEMENTS OF THE SIMPLE PENDULUM SENSING AND DRIVING MATRICES CORRESPONDING TO THE 95% CONFIDENCE LEVEL.

	$\mathcal{S}_{11}$	$\mathcal{S}_{12}$	$\mathcal{D}_{11}$	$\mathcal{D}_{12}$
max	0.9975	0.0696	0.6204	0.6380
min	0.9976	0.0707	0.6218	0.6427
	$\mathcal{S}_{21}$	$\mathcal{S}_{22}$	$\mathcal{D}_{21}$	$\mathcal{D}_{22}$
max	−0.1819	0.9819	0.8266	−0.8096
min	−0.1893	0.9833	0.8284	−0.8159

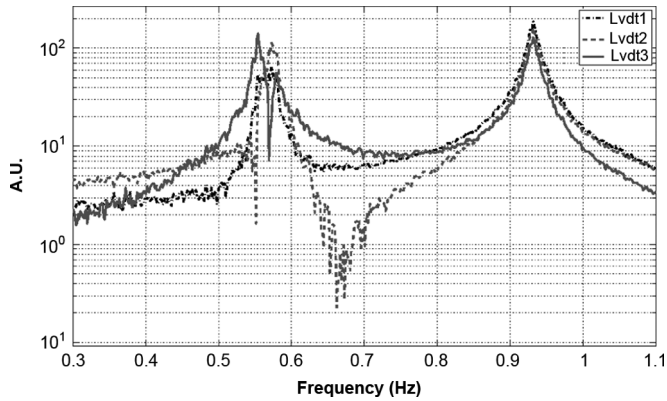

Fig. 9. Real LVDT transfer function obtained exciting the system by means of real actuator (Coil 3). The translational peaks (0.55 Hz and 0.58 Hz) are quasi-degenerate.

An example of non diagonalized system is shown in figure (9). In the same figure it is possible to notice the quasi-degeneration in the translational modes.

Using the method described in the previous section, we have found the LVDT sensing matrix $\mathcal{S}$:

$$\begin{pmatrix} L_x \\ L_z \\ L_{R\theta} \end{pmatrix} = \begin{pmatrix} -0.556 & -0.045 & 0.83 \\ 0.357 & -0.798 & 0.486 \\ -0.829 & -0.526 & -0.188 \end{pmatrix} \cdot \begin{pmatrix} L_1 \\ L_2 \\ L_3 \end{pmatrix}$$

and the driving matrix $\mathcal{D}$:

$$\begin{pmatrix} C_1 \\ C_2 \\ C_3 \end{pmatrix} = \begin{pmatrix} 0.0002 & -0.816 & 0.591 \\ 0.528 & 0.4903 & 0.783 \\ -0.868 & 0.306 & 0.265 \end{pmatrix} \cdot \begin{pmatrix} C_x \\ C_z \\ C_{R\theta} \end{pmatrix}.$$

The diagonalization results obtained (sensing and driving matrices) can be experimentally evaluated and compared with the diagonalization procedure prediction. Such a prediction is simply obtained combining real actuator and real sensor signals using driving and sensing matrices. This comparison is shown in Fig. 10.

Table II reports the upper and lower limits for the elements of the IP $\mathcal{S}$ and $\mathcal{D}$ matrices corresponding to the 95% confidence level.

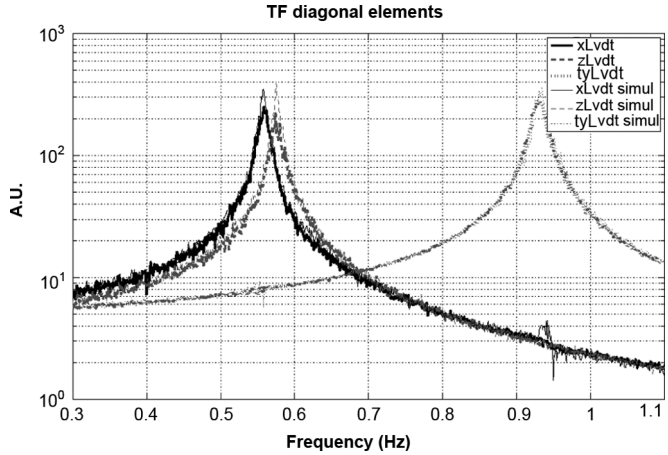

Fig. 10. Transfer function comparison between measurements results and predicted behavior obtained using diagonalization procedure results (*simul* in the label).

TABLE II
UPPER AND LOWER LIMITS FOR THE ELEMENTS OF THE IP SENSING AND DRIVING MATRICES CORRESPONDING TO THE 95% CONFIDENCE LEVEL.

	$\mathcal{S}_{11}$	$\mathcal{S}_{12}$	$\mathcal{S}_{13}$	$\mathcal{D}_{11}$	$\mathcal{D}_{12}$	$\mathcal{D}_{13}$
max	-0.552	-0.040	0.827	0.005	-0.814	0.587
min	-0.559	-0.049	0.832	-0.005	-0.819	0.595
	$\mathcal{S}_{21}$	$\mathcal{S}_{22}$	$\mathcal{S}_{23}$	$\mathcal{D}_{21}$	$\mathcal{D}_{22}$	$\mathcal{D}_{23}$
max	0.352	-0.795	0.482	0.524	0.486	0.779
min	0.361	-0.800	0.490	0.532	0.494	0.787
	$\mathcal{S}_{31}$	$\mathcal{S}_{32}$	$\mathcal{S}_{33}$	$\mathcal{D}_{31}$	$\mathcal{D}_{32}$	$\mathcal{D}_{33}$
max	-0.827	-0.521	-0.183	-0.866	0.301	0.260
min	-0.832	-0.530	-0.193	-0.870	0.310	0.269

Analyzing the values in Table I it results that all the errors affecting the elements of the matrices $\mathcal{S}$ and $\mathcal{D}$ are below 1%, except for $\mathcal{S}_{12}$ and $\mathcal{S}_{21}$. In the case of Table II, instead, the errors on the matrix elements are below 5% but for $\mathcal{S}_{21}$, $\mathcal{S}_{33}$ and $\mathcal{D}_{11}$. In particular the value found for this last element is consistent with zero, and indicates that the actuation along the x axis does not need to use the C_1 actuator. This means that the x axis results to be orthogonal to the direction of the force exerted by C_1.

In both cases the effect of the errors affecting the matrix elements was estimated by computing the following quantity:

$$\mathcal{E}_{ij}^{\min} = \frac{\int \left[\mathcal{H}_{ij}^{\min}(f) - \mathcal{H}_{ij}(f)\right] \mathrm{d}f}{\int \mathcal{H}_{ij}(f) \mathrm{d}f} \tag{11}$$

$$\mathcal{E}_{ij}^{\max} = \frac{\int \left[\mathcal{H}_{ij}^{\max}(f) - \mathcal{H}_{ij}(f)\right] \mathrm{d}f}{\int \mathcal{H}_{ij}(f) \mathrm{d}f} \tag{12}$$

where the integrals were calculated on the whole frequency range used to estimate the experimental transfer functions, and the matrices $\mathcal{H}^{\min}$ and $\mathcal{H}^{\max}$ are

$$\mathcal{H}^{\min} = \mathcal{S}^{\min} \cdot \mathcal{R} \cdot \mathcal{D}^{\min} \tag{13}$$

$$\mathcal{H}^{\max} = \mathcal{S}^{\max} \cdot \mathcal{R} \cdot \mathcal{D}^{\max} \tag{14}$$

and the $\mathcal{S}^{\min}$, $\mathcal{D}^{\min}$, $\mathcal{S}^{\max}$, $\mathcal{D}^{\max}$ matrices are obtained from the corresponding $\mathcal{S}$ and $\mathcal{D}$ matrices, by substituting all their elements by the minimum and maximum values in the respective confidence interval.

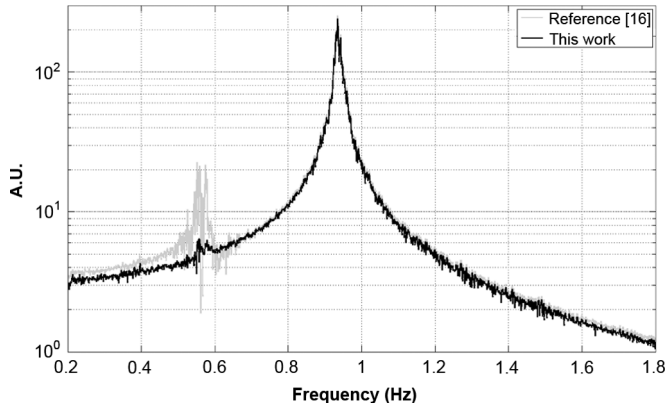

Fig. 11. Comparison of ty/C_1 transfer functions as computed with the procedure described in this work and with the procedure described in [16].

The matrices $\mathcal{E}^{\min}$ and $\mathcal{E}^{\max}$ give a rough estimate of the deviation induced by the errors on all the elements of $\mathcal{H}$. For both applications all their elements are below 5%; in particular all the diagonal elements are below 0.5% indicating the low impact of the errors on the results.

A comparison of the performances of this procedure can be done only with the sensing matrix $\mathcal{S}$ as calculated with the procedure described in [16]. The outcome of the comparison is shown in Fig. 11 for the ty virtual sensor when actuation is performed using the C_1 coil. From the figure is clear that our procedure produce a better uncoupling, since the other transfer function shows a larger residual structure around the resonance frequencies of the x and z degrees of freedom. Other degrees of freedom behave similarly. More direct comparisons are not possible since the other procedure requires a second set of measurements to compute the driving matrix.

VI. CONCLUSIONS

In this paper we have examined a numerical procedure to diagonalize a MIMO system. Preliminary tests, performed on a simpler system have been successful. The same procedure has been extensively used on a more complex mechanical system. The method developed and previously described offers the advantage to rely only on direct measurements without requiring a detailed model of the system. As a consequence of this characteristic, it can be easily adopted in complex system which presents some difficulties into determining a perfect model to describe the system response (obviously if degrees of freedom are not intrinsically entangled).

This point makes such a method very flexible and suitable to be applied in different physical systems. Especially systems in which could be difficult to find a correct model to describe them.

But this is not the only advantage showed by this method. In addition:

- it does not require two distinct steps to obtain sensing and driving matrices (as usually done in VIRGO, TAMA, etc.);
- it works even with quasi-degenerate systems.

REFERENCES

[1] T. Accadia *et al.*, "Status and perspectives of the Virgo gravitational wave detector," in *J. Phys.: Conf. Ser.*, 2010, vol. 203, p. 012074.

[2] LIGO Laser Interferometer Gravitational-Waves Observatory. [Online]. Available: http://www.ligo.caltech.edu
[3] GEO600 The German-British Gravitational Wave Detector. [Online]. Available: http://geo600.aei.mpg.de/
[4] M. Ando *et al.*, "Current status of the TAMA300 gravitational-wave detector," *Class. Quantum Grav.*, vol. 22, p. S881, 2005.
[5] D. H. Owens, "Dyadic expansion for the analysis of linear multivariable systems," *Proc. IEEE*, vol. 121, no. 7, pp. 713–716, 1974.
[6] G. Losurdo *et al.*, "An inverted pendulum preisolator stage for the VIRGO suspension system," *G. Losurdo Rev. Sci. Instr.*, vol. 70, pp. 2507–2515, 1999.
[7] A. Giazotto, U. Bruzzo, R. Cianci, and E. Massa, Eds., in *Proc. 7th Conf. General Relativity and Gravitational Physics*, 1987, pp. 449–463.
[8] D. Shoemaker *et al., Phys. Rev. D*, vol. 38, pp. 423–432, 1988.
[9] R. Weiss, Progress Report No. 105, MIT Quart., 1972.
[10] G. Cella *et al.*, "Monolithic geometric anti-spring blades," *Nucl. Instrum. Methods Phys. Res. A*, vol. 540, pp. 502–519, 2005.
[11] F. Acernese *et al.*, "First locking of the Virgo central area interferometer with suspension hierarchical control," *Astropart. Phys.*, vol. 20, pp. 629–640, 2004.
[12] H. Tariq *et al.*, "The linear variable differential transformer (LVDT) position sensor for gravitational wave interferometer low-frequency controls," *Nuc. Instr. Meth. A*, vol. 489, pp. 570–576, 2002.
[13] F. Acernese, F. Barone, R. De Rosa, L. Milano, K. Qipiani, and F. Silvestri, "Digital control system for mechanical damping of suspended mass," *Proc. SPIE*, vol. 5052, p. 451, 2003.
[14] R. De Rosa, F. Garufi, L. Milano, S. Mosca, and G. Persichetti, "Characterization of electrostatic actuators for suspended mirror control with modulated bias," in *J. Phys.: Conf. Ser.*, 2010, vol. 228, p. 012018.
[15] C. Wang, H. Tariq, R. DeSalvo, Y. Iida, S. Marka, Y. Nishi, V. Sannibale, and A. Takamori, "Constant force actuator for gravitational wave detector's seismic attenuation systems (SAS)," *Nuc. Instr. Meth. Phys. Res. A*, vol. 489, pp. 563–569, 2002.
[16] G. Losurdo *et al.*, "Inertial control of the mirror suspensions of the VIRGO interferometer for gravitational wave detection," *Rev. Sci. Instrum.*, vol. 72, pp. 3653–3661, 2001.
[17] A. Gennai, S. Mancini, T. Maiani, and D. Passuello, VIRGO Internal Report No. VIR-NOT-PIS-1390-101, 1997.
[18] G. Losurdo, ""Ultra-low frequency inverted pendulum for the VIRGO test mass suspension," Ph.D. dissertation, Scuola Normale Superiore, Pisa, Italy, 1998 [Online]. Available: https://wwwcascina.virgo.infn.it/theses/DottLosurdo.ps
[19] T. F. Coleman and Y. Li, "An interior, trust region approach for nonlinear minimization subject to bounds," *SIAM J. Optimization*, vol. 6, pp. 418–445, 1996.
[20] G. A. F. Seber and C. J. Wild, *Nonlinear Regression*. New York: Wiley, 1989.